# Scaling analysis of bio-molecular dynamics derived from elastic incoherent neutron scattering experiments

W. Doster, H. Nakagawa, and M. S. Appavou

Citation: J. Chem. Phys. **139**, 045105 (2013); doi: 10.1063/1.4816513
View online: http://dx.doi.org/10.1063/1.4816513
View Table of Contents: http://jcp.aip.org/resource/1/JCPSA6/v139/i4
Published by the AIP Publishing LLC.

# Scaling analysis of bio-molecular dynamics derived from elastic incoherent neutron scattering experiments

W. Doster,[1,a)] H. Nakagawa,[2,3] and M. S. Appavou[2]
[1]*Physik-Department, Technische Universität München, D-85748 Garching, Germany*
[2]*Jülich Centre for Neutron Science, Forschungszentrum Jülich GmbH, Outstation at MLZ, Lichtenbergstraße 1, 85747 Garching, Germany*
[3]*Japan Atomic Energy Agency, Quantum Beam Science Directorate, Tokai, Ibaraki 319-1195, Japan*

(Received 27 March 2013; accepted 10 July 2013; published online 31 July 2013)

Numerous neutron scattering studies of bio-molecular dynamics employ a qualitative analysis of elastic scattering data and atomic mean square displacements. We provide a new quantitative approach showing that the intensity at zero energy exchange can be a rich source of information of bio-structural fluctuations on a pico- to nano-second time scale. Elastic intensity scans performed either as a function of the temperature (back-scattering) and/or by varying the instrumental resolution (time of flight spectroscopy) yield the activation parameters of molecular motions and the approximate structural correlation function in the time domain. The two methods are unified by a scaling function, which depends on the ratio of correlation time and instrumental resolution time. The elastic scattering concept is illustrated with a dynamic characterization of alanine-dipeptide, protein hydration water, and water-coupled protein motions of lysozyme, per-deuterated c-phycocyanin (CPC) and hydrated myoglobin. The complete elastic scattering function versus temperature, momentum exchange, and instrumental resolution is analyzed instead of focusing on a single cross-over temperature of mean square displacements at the apparent onset temperature of an-harmonic motions. Our method predicts the protein dynamical transition (PDT) at $T_d$ from the collective ($\alpha$) structural relaxation rates of the solvation shell as input. By contrast, the secondary ($\beta$) relaxation enhances the amplitude of fast local motions in the vicinity of the glass temperature $T_g$. The PDT is specified by step function in the elastic intensity leading from elastic to viscoelastic dynamic behavior at a transition temperature $T_d$. © *2013 AIP Publishing LLC*. [http://dx.doi.org/10.1063/1.4816513]

## I. INTRODUCTION

Neutron spectroscopy is a useful technique to address the nature of fast structural fluctuations in bio-molecules and of hydration water on a pico- to nano-second time scale. Useful summaries are given in several articles.[1–5] To collect data with sufficient statistical accuracy at low neutron flux covering the full spectral range is time consuming and involves a complicated numerical analysis. This limitation is particularly relevant if a wide range of experimental parameters such as temperature or solvent conditions have to be examined. Thus, numerous neutron scattering studies with biological background focus on the narrow elastic spectral range at zero energy exchange, where the scattering intensity is at the maximum.[6–22] From the variation of the elastic intensity versus momentum exchange and temperature, mean square displacements (MSD) are derived. A common qualitative explanation of dynamic processes occurring within the bio-molecule approximates the MSD versus the temperature by straight lines. The slopes are interpreted as force constants and the cutting edge between the two slopes is assigned to onset temperatures of dynamic processes, $T_{on}$, depending on the particular model.[10,16,19,20,22]

The logic of this procedure is based on particle conservation and the fact that the total scattering power is only weakly depending on experimental conditions: The total number of scattered neutrons per time interval is constant, independent of the scattering parameters. This gives rise to a sum rule, which states that any decrease in the elastic scattering fraction is compensated by an equivalent increase in the inelastic spectral area.[23] This indirect approach to molecular motions derived from the elastic intensity of the spectrum, which reflects the rigid aspects of the bio-molecule, seems counterintuitive. It is thus important to clarify both, the theoretical and experimental basis of the information, which can be deduced from the elastic intensity.

Dedicated elastic scans versus temperature using a fixed energy window are easy to perform with back-scattering (BS) instruments. This method has become quite popular, focusing on the onset of an-harmonic motions in proteins, which is often identified with the "protein dynamical transition" (PDT).[7] At the onset temperature $T_{on}$, where the time scale of molecular motions becomes comparable to the instrumental resolution time $\tau_{res}$, a drastic decrease in the elastic intensity is observed.[7,24] The PDT derived from elastic scattering intensities has received several conflicting explanations.[25] For instance, it was interpreted as a structural change of protein hydration water, leading to a fragile to strong cross-over in the Arrhenius plot of the average relaxation times.[26,23]

a)Author to whom correspondence should be addressed. Electronic mail: wolfgang.doster@ph.tum.de. Tel.: (+49) 8122903562.

 

In a recent publication, Magazu *et al.*[18] propose to use this cross-over at various instrumental resolutions as a general method (RENS), to determine the average relaxation time $\langle\tau_c\rangle$ versus the temperature $T_{on}$. Several theoretical studies discuss the effect of instrumental resolution on the elastic intensity and elastic mean square displacements.[27–29]

Our goal from the beginning was to reconstruct from the elastic intensity the complete dynamic information. In two publications 2001 and 2003, we have shown that room temperature protein dynamics can be derived from elastic scattering data using a method called ERS (elastic resolution spectroscopy).[30,31] With ERS it was demonstrated that the restrictions, imposed by collecting data covering a limited spectral range, can be overcome by performing experiments at any fixed temperature, while changing the instrumental resolution. The PDT could thus be studied at physiological temperatures: Two dynamic components were observed: (1) rotational transitions of methyl groups in hydrated myoglobin and (2) water coupled structural fluctuations.[30,31] This is technically possible with current time-of-flight (TOF) neutron spectrometers by continuously varying the chopper speed: TOF employs two chopper systems to select the wavelength of the incoming neutrons and to analyze the energy transfer of the scattered beam. So far, the ERS method was applied with the TOF instruments IN5 (ILL in Grenoble) and V3 at the Hahn Meitner Institute in Berlin.[30,31]

ERS yields, at least in principle, the same type of dynamic information as with a standard QENS (quasi-elastic neutron scattering) setup. Some common properties with the spin-echo technique are discussed in Ref. 31. Although the QENS spectral analysis is to be preferred in standard situations, there are a number of properties which render ERS attractive for special cases:

(1) For weakly scattering samples, only the strong elastic intensity may be evaluated with sufficient statistical accuracy. Many biological samples are available only in small quantities (mg), which exclude any spectral analysis with conventional QENS, requiring 100-200 mg. Moreover, per-deuterated samples exhibit a much lower cross-section than native molecules.
(2) Small dynamic changes as a result of structural transitions in bio-molecules will mainly affect the elastic intensity, where the total loss is concentrated, while the gain in quasi-elastic intensity is distributed over the noisy spectral wings.[31]
(3) In contrast to fixed resolution QENS, the ERS experiment is designed to systematically scan a wide range of instrumental resolutions, meV to $\mu$eV, which is quite useful to characterize complex spectra. With TOF-ERS the instrumental resolution can be varied by nearly 3 decades with current spectrometers.
(4) The information is obtained directly in the time domain as an approximation of the "intermediate scattering function," which avoids the numerical Fourier transform of noisy spectral data.
(5) Most elastic scattering experiments with bio-molecules were performed as elastic scans versus the temperature using back-scattering instruments at fixed resolution. The average relaxation time can be extracted from the onset temperature $T_{on}$ of the relaxation process.[18]

It will be demonstrated, that by fitting the complete elastic temperature scan, one can extract in addition the activation energy and the pre-exponential, if the shape of the spectrum is known.[24,25] Moreover, even the shape of the relaxation time spectrum can be determined, if the temperature scans are performed at two different instrumental resolutions. This approach extends the range of application of classical TOF-ERS to back-scattering spectrometers. To explore the new possibilities of back-scattering with ERS is one of the main goals of this article. Finally, a variety of misconceptions exist about the interpretation of elastic scattering intensities and the derivation of atomic mean square displacements, which will be clarified.[25] We show how the PDT can be predicted on a quantitative basis using solvent relaxation data.

## II. THE RELATION BETWEEN ELASTIC (ENS) AND QUASI-ELASTIC NEUTRON SCATTERING

In a standard QENS experiment, one collects spectral data at fixed instrumental resolution until sufficient statistical accuracy, compatible with the allocated beam time, is achieved across the low intensity spectral wings. In the ERS experiment, one collects data with sufficient accuracy in the high intensity elastic region for a much shorter time at a particular resolution, which is then adjusted to a new value. Fig. 1 shows an example of a QENS experiment, performed at the NEAT time-of-flight spectrometer (BENSC, Berlin) at a nominal instrumental energy resolution (full width at half maximum (FWHM)) of 48 $\mu$eV.[31]

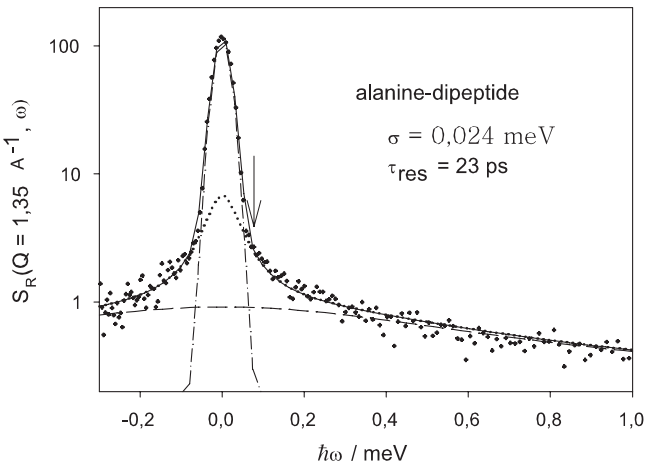


FIG. 1. Scattering function of alanine dipeptide at $Q = 1.35$ Å$^{-1}$ (dots) taken at an incident neutron wavelength of 8 Å and a chopper speed of 5000 rpm (NEAT). Instrumental resolution FWHM: 0.048 meV, corresponding to a resolution time of 23 ps. The full line represents a fit assuming three spectral components: (1) the narrow Gaussian spectrum represents the ERS fit to derive the elastic intensity (dashed-dotted). (2) The broad Lorentzian spectrum (dashed) corresponds to the rotational motion of the methyl groups, (3) the narrow line (dotted) suggests a further slow reorientational process associated with the axis of the peptide.[31] The arrow indicates the intensity at $\omega = 3\sigma$, which has to be subtracted from the elastic intensity at $\omega = 0$ to correct for the quasi-elastic scattering (Eq. (40)).

A powder sample of alanine-dipeptide crystals was investigated, which is one of the simplest model systems with interactions resembling those occurring in proteins. The dynamic spectrum, which has also been investigated by molecular dynamic simulations,[51] is dominated by rotational motions of two terminal (C- and N-) methyl groups and the methyl side-chain of alanine. The elastic intensity rises up to 110 units, while the intensity of the broad quasi-elastic line reflecting the rotational dynamics of methyl groups is lower by a factor of 100 (note the logarithmic intensity scale). To collect data of this quality requires typically 6 h of beam time with a large amount (300 mg) of sample. For the elastic peak less than 30 min would be sufficient. Obviously, the chosen instrumental resolution is not adequate to map the broad quasi-elastic spectrum of the three methyl groups. Moreover, the spectrum contains an additional narrow quasi-elastic line, which is only partially resolved by the spectrometer. This result illustrates that the standard QENS approach with fixed resolution is not optimal if the spectrum of relaxation times covers a wide range.

In Sec. III, we discuss the theoretical background of incoherent elastic neutron scattering experiments.

## III. THEORETICAL BACKGROUND OF ELASTIC INCOHERENT NEUTRON SCATTERING (EINS)

### A. Cross sections of hydrated proteins

Biomolecules are hydrogenous organic compounds. The unique relevant isotope is thus the hydrogen atom, which exhibits the largest neutron cross section of all nuclei, 80.2 b (1 barn (b) = $10^{-24}$ cm$^2$). The total cross sections of carbon (5.56 b), oxygen (4.2 b), and nitrogen (11.5 b) are much lower,[32] which, for dehydrated native proteins, results in a 90% hydrogen scattering fraction.[33] Water, the major solvent, contains two hydrogen atoms per molecule. Due to the large number of water molecules even in highly concentrated protein solutions, the total scattering cross section by water will be overwhelming. This is one of the main reasons, why proteins are studied at low water content in a hydrated state instead of in solution. Deuterium (D) by contrast exhibits a much lower total cross section than hydrogen (7.6 b). To investigate protein dynamics with neutron spectroscopy, $H_2O$ is often replaced by $D_2O$ using hydrated samples or concentrated solutions. Another important point is the distinction between two types of cross sections: (1) phase-preserving or coherent cross section, $\sigma_{\mathrm{coh}}$ and (2) phase-destructive or incoherent cross section, $\sigma_{\mathrm{inc}}$. The incoherent component results from spin disorder, modulating the spin dependent cross section. The incoherent cross section of hydrogen (I = 1/2) interacting with neutrons (I = 1/2), which are randomly polarized is much larger (80.26 b) than the coherent part (1.76 b). As a result, scattered neutron waves, originating from different hydrogen atoms in the molecule interfere with random phases. Only the "self-scattering" of waves originating from one and the same nucleus shifted in time produce regular interference patterns on the detector. The self-scattering part thus reflects the single particle displacement in time and space, while the coherent part derives from collective relative particle displacements. Diffusion and relaxation of density fluctuations can be studied with incoherent scattering, while collective excitations, dispersion of phonons, can be observed only with coherent scattering. Deuterium by contrast exhibits a coherent cross section of 5.6 b (similar to C or O), while $\sigma_{\mathrm{inc}}$ (D) = 2.04 b is 40 times lower than the value for hydrogen. But it is incorrect to assume a factor of 40 (instead of 10) to represent the ratio of protein to $D_2O$-scattering, ignoring the coherent fraction originating from $D_2O$ and the non-hydrogen atoms of the protein.[33] In the scattering experiment, one is measuring the momentum exchange $\hbar\,\mathbf{Q} = \hbar\,(\boldsymbol{k} - \mathbf{k}_0)$, the difference between the initial and final value of the wave vectors $\mathbf{k_0}$ and $\mathbf{k}$ and the energy exchange $E - E_0 = \hbar\omega$, between the neutron probe and the molecules in the sample. The scattered neutron flux $j_s(\theta, \phi)$ is recorded in a particular direction with momentum, $\mathbf{k}(\theta, \phi)$, covering a solid angle interval between $\Omega$ and $\Omega + d\Omega$ and a frequency interval, between $\omega$, $\omega + d\omega$. The neutron flux is given by $\mathbf{j} = n \cdot \mathbf{v} = n/m\,\hbar\,\mathbf{k}$ [cm$^{-2}$ s$^{-1}$], in terms of the number density of neutrons n [cm$^{-3}$] and the neutron velocity $\mathbf{v}$ [cm s$^{-1}$]. The scattered flux $j_s(\mathbf{k},E)$ normalized by the incident flux $j_0(\mathbf{k}_0, E_0)$, solid angle- and the frequency interval, yields the double differential cross section $\frac{\partial^2\sigma}{\partial\Omega\partial\omega}$. For a single isotope like hydrogen, the double differential cross section is composed of two parts originating from coherent and incoherent scattering[32,34,35]

$$\frac{\partial^2\sigma}{\partial\Omega\partial\omega} = \frac{j}{j_0}\frac{1}{d\Omega d\omega} = \frac{N}{4\pi}\frac{k}{k_0}[\sigma_{coh}S_{coh}(Q,\omega) + \sigma_{inc}S_{inc}(Q,\omega]. \quad (1)$$

$S_{\mathrm{coh}}(Q,\omega)$ and $S_{\mathrm{inc}}(Q,\omega)$ are the coherent and incoherent scattering functions related to the N atoms of a particular isotope in the sample. Note that the factor N appears in the numerator and not in the denominator as in Eq. (2.47) of Bee[32] and Eq. (14) of Gabel *et al.*[28] The ratio $k/k_0$ appears in Eq. (1), since the flux is proportional to the neutron momentum $\hbar k = mv$, m denotes the neutron mass. Equation (1) implies that a scattering function exists for each atom, while all atoms are assumed to be dynamically equivalent. This is only correct if the environments are also equivalent. In the case of hydrated proteins, one has account for at least four different hydrogen environments: (1) the methyl protons (25% of the total cross section), (2) other non-exchangeable side-chain protons, (3) the exchangeable protons (NH or polar side chain protons), and (4) the hydration water protons. Apart from hydrogen, the coherent scattering from other atoms C, O, and N have to be taken into account. One has to sum over the protons of different environments $\alpha$ for each nucleus of type $\beta$, which yields instead of Eq. (1)

$$\frac{\partial^2\sigma^{tot}}{\partial\Omega\partial\omega} = \frac{N\cdot k}{4\pi\cdot k_0}\sum\nolimits_{\alpha,\beta}\left[\sum\nolimits_{\beta'}\sqrt{\sigma^{\beta}_{coh}\sigma^{\beta'}_{coh}}S^{\alpha\beta\beta'}_{coh}(Q,\omega) + \sigma^{\beta}_{inc}S^{\alpha\beta}(Q,\omega)\right]. \quad (2)$$

To separate the coherent and incoherent scattering functions requires a polarization analysis of the scattered neutrons, requiring special instruments. This type of experiment was

performed only recently for several proteins and various solvent conditions over the relevant Q-range by Gaspar *et al.*[33] The experiments demonstrate that about 80% of the scattering cross section of $D_2O$-hydrated proteins is incoherent above Q = 0.3 Å$^{-1}$, at lower Q-values however, coherent scattering dominates. This result complicates the extrapolation of elastic scattering data to low Q values, required to derive mean square displacements. In the following, we focus on the elastic incoherent part of the scattering function and specialize first to a single class of protons, $S_{inc}(Q, \omega)$. This restriction is given up in Sec. IV. At $\omega = 0$, the spectral functions are reduced to $S_{inc}(Q, 0) = EISF(Q)\ \delta(\omega)$. $\delta(\omega)$ is the $\delta$-function and the EISF(Q) denotes elastic incoherent structure factor. From the EISF, one can deduce the spatial arrangement of dynamically accessible states. Note that a similar relation exists for the coherent scattering fraction: $S_{coh}(Q,0) = S_{coh}(Q)\ \delta(\omega)$ where $S_{coh}(Q)$ denotes the coherent structure factor.

### B. The elastic fraction versus elastic intensity and the scaling function

Due to the nearly rigid native structure of bio-molecules, where the position of most atoms within the molecule is confined to a narrow range, an intense elastic scattering profile is produced. From the coherent fraction of the elastic scattering function of protein crystals, $S_{coh}(Q)$, one determines the 3D neutron structure of the molecule.[36] A different kind of information is obtained from the incoherent elastic scattering fraction, termed the "incoherent elastic structure factor," EISF(Q). In contrast to the coherent structure factor $S_{coh}(Q)$, which is dominated by inter-atomic correlations and average positions, the EISF(Q) reflects self-correlations and thus fluctuations about the average structure. The incoherent method profits from the large incoherent scattering cross section of the hydrogen nucleus, which is about 10 times larger than the combined coherent and incoherent cross section of carbon, nitrogen, oxygen, or deuterium. The total scattering cross section of $D_2O$-hydrated proteins is thus dominated (80%–90%) by proton-incoherent scattering.[33] The contribution of the deuterated solvent increases with concentration and may eventually dominate the quasi-elastic spectrum due to its high mobility. As opposed to single crystals, the samples studied in such incoherent scattering experiments are generally isotropic: protein solutions, hydrated powders, or polycrystalline material. The incoherent structure factor is thus averaged covering all orientations of the molecules, which is called the "powder average."

Another important feature of the incoherent structure factor is the normalization at Q = 0, thus EISF(Q = 0) ≡ 1. The EISF(Q) contains information about the geometry of single particle displacements as defined by the long-time self-displacement distribution function $G_s(\mathbf{r},t)$[32,34,35]

$$EISF(Q) = \left\langle \int d^3\vec{r} e^{-i\vec{Q}\vec{r}} G_s(\vec{r}, t \to \infty) \right\rangle_{powder}. \quad (3)$$

$G_s(\mathbf{r},t)$, ignoring quantum effects, denotes the conditional probability $p(r_0, r_0 + r, t)$, averaged over all initial positions, $\mathbf{r}_0$, that a particle has moved from $\mathbf{r}_0$ during time interval t across a distance **r**

$$G_s(\vec{r}, t) = \int d^3 r_0 p_o(\vec{r}_0) p(\vec{r}_0, \vec{r}_0 + \vec{r}, t). \quad (4)$$

Its Fourier transform at finite times denotes the self-intermediate scattering function $I_s(Q, t)$ according to Eqs. (3) and (4)

$$I_s(Q, t) = \left\langle \int d^3\vec{r} e^{-i\vec{Q}\vec{r}} G_s(\vec{r}, t) \right\rangle_{powder}. \quad (5)$$

Note that Eqs. (2.218) and (2.220a) of Bee[32] use d**r** instead of $d^3\mathbf{r}$, which could be misunderstood as a displacement instead of a volume element.

Often it is useful to split the intermediate scattering function into a time-dependent component F(Q, t) with $F(Q, t \to \infty) = 0$ and a time-independent part, the EISF(Q) according to

$$I_s(Q, t) = [1 - EISF(Q)]\, F(Q, t) + EISF(Q). \quad (6)$$

The EISF(Q) is also known as the "elastic fraction" of the spectrum, since in the frequency domain it is the source of elastic scattering. The complementary quantity 1 − EISF(Q) = QEISF(Q) is often called the "quasi-elastic fraction" of the spectrum taken in the frequency domain. The Fourier transform of Eq. (6) then reads

$$S_{inc}(Q, \omega) = EISF(Q) \cdot \delta(\omega) + QEISF(Q) \cdot S_{qel}(Q, \omega). \quad (7)$$

$S_{qel}(Q,\omega)$ is the quasi-elastic component of the spectrum, the Fourier transform of F(Q, t). In the case of spatially unrestricted displacements, such as long range diffusion, $G(\mathbf{r}, t \to \infty)$ vanishes at long times, thus $EISF^{Diff}(Q) \equiv 0$. A liquid can be discriminated dynamically from a solid, where the molecules are localized, by the glass form factor $f_c(Q)$

$$EISF(Q) = \begin{cases} f_c(Q) = 0 & \text{liquid state: long range diffusion} \\ f_c(Q) > 0 & \text{solid or glassy state: localized motion} \end{cases}. \quad (8)$$

The liquid-glass transition then reveals itself by an abrupt change of $f_c = 0$ to a finite value > 0 at a particular temperature $T_d$.[37–39] Three further corrections need to be taken into account: $S_{inc}(Q, \omega)$ has to be convoluted (*) with the vibrational spectrum $S_{vib}(Q, \omega)$. Since the oscillations are fast and generally well resolved, the vibrational correction reduces to a multiplication of the spectrum with the vibrational Debye Waller factor

$$S_{inc}^{tot}(Q, \omega) = S_{inc}(Q, \omega)^* S_{vib}(Q, \omega) \approx \exp(-Q^2 \langle \Delta x_{vib}^2 \rangle) \cdot S_{inc}(Q, \omega). \quad (9)$$

$\langle \Delta x_{vib}{}^2 \rangle$ denotes the 1D vibrational mean square displacement. Second, we deal only with single scattering, assuming that the cross-section is low enough to ignore multiple scattering. This implies that the transmission of the sample must be larger than 90%.[52,56]

Third, $S_{inc}(Q,\omega)$ has to be convoluted with the instrumental resolution function.

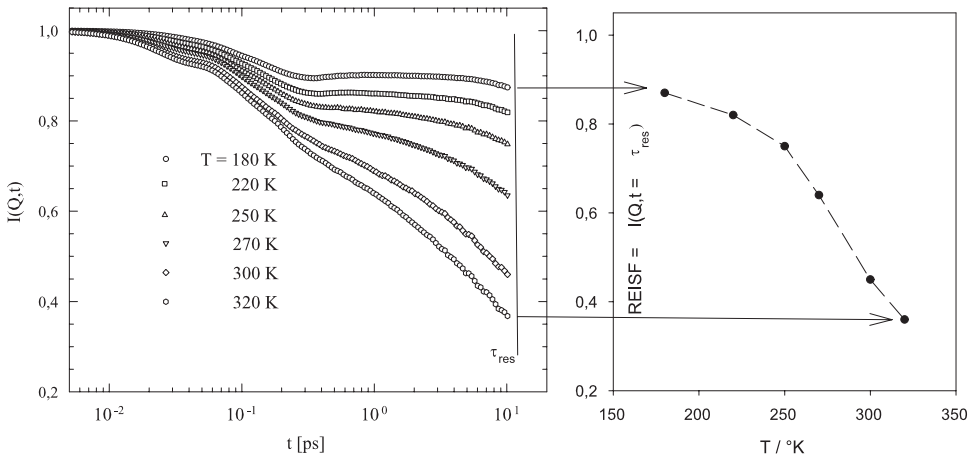


FIG. 2. (a) Temperature dependent intermediate scattering function I(Q,t) of hydration water (hydrated myoglobin 0.35 g/g) deconvoluted from the instrumental resolution with $\tau_{res} \approx 12$ ps at Q = 1.8 $A^{-1}$. The displayed data are the result of a numerical Fourier transform of $\Delta S(Q, \omega)$, which denotes the difference spectrum of $H_2O$- and $D_2O$-hydrated myoglobin (IN6, ILL, Grenoble). (b) The resulting elastic fraction REISF ($t = \tau_{res}$) versus the temperature (arrows) is also shown.

Taking into account the finite instrumental width, $\Delta\omega$, useful information is obtained only up to a maximum observation time $\tau_{res} \approx 1/\Delta\omega$. Instead of the EISF(Q) of Eq. (3), one measures a resolution dependent elastic fraction REISF(Q, $\tau_{res}$)

$$REISF(Q, \tau_{res}) = \left\langle \int d^3\vec{r} e^{-i\vec{Q}\vec{r}} G_s(\vec{r}, t \approx \tau_{res}) \right\rangle_{powder}. \tag{10a}$$

Thus, an excess elastic fraction, REISF(Q, $\tau_{res}$) − EISF(Q) ≥ 0, is produced due to apparently localized particles, if the particle displacements are probed with insufficient resolution. The resulting resolution-limited displacements will then appear finite even for unconstrained motion. The apparent elastic fraction REISF(Q, $\tau_{res}$), as a function of $t = \tau_{res}$, contains the full dynamic information equivalent to the powder-averaged intermediate scattering function I(Q, t). From Eqs. (6) and (10a), it follows that

$$REISF\,(Q, \tau_{res}) \equiv I_s\,(Q, t = \tau_{res})\,. \tag{10b}$$

Fig. 2(a) shows an example of a de-convoluted intermediate scattering function of protein hydration water adsorbed at myoglobin versus time and temperature. The instrumental resolution time of the TOF spectrometer IN6 at the ILL in Grenoble was $\tau_{res} \cong 15\ (\pm 2)$ ps. The spectra were initially collected in the frequency domain, then the data were Fourier-transformed numerically to the time domain.[1,40] The result was finally de-convoluted from the instrumental resolution function. Fig. 2(b) shows the resulting values of the apparent elastic fraction REISF(Q = 1.8 $Å^{-1}$, T) = $I_s$(Q, t = $\tau_{res}$ = 12 ps) at different temperatures. The non-vanishing value of $I_s(Q, t \cong \tau_{res})$ produces a finite apparent elastic fraction. The derivation of the **apparent elastic fraction** REISF requires a complete inelastic, model-dependent analysis, separating elastic from quasi-elastic spectral components, followed by the de-convolution of the spectra from the instrumental resolution function. The **elastic fraction** is thus different from the **elastic intensity**.

We have demonstrated, however, within the framework of "elastic resolution spectroscopy," that, at least approximately, the same dynamic information can be extracted from the elastic intensity at $\omega = 0$, which is taken directly from the spectrum without a sophisticated spectral analysis.

TOF and back-scattering experiments are performed in the frequency domain. It is then straightforward to record the intensity of the scattering function $S_{inc}(Q, \omega)$ at $\omega = 0$ as $I_{el}(Q) = S_{inc}(Q, \omega = 0)$. The true spectrum is generally convoluted with the instrumental resolution function $R'(\omega,\Delta\omega)$, where $\Delta\omega$ parameterises the resolution width. Energy resolved neutron scattering experiments thus yield a frequency dependent scattering function $S_R(Q, \omega, \Delta\omega = 1/\tau_{res})$ according to

$$S_R(Q, \omega, \Delta\omega) = \int_{-\infty}^{\infty} d\omega' R'(\omega - \omega', \Delta\omega) S_{inc}(Q, \omega). \tag{11}$$

Equivalently, one can write Eq. (11) as a Fourier transform of the respective functions in the time domain

$$S_R(Q, \omega, \Delta\omega) = \frac{1}{2\pi} \int_{-\infty}^{\infty} dt e^{-i\omega t} R(t, \tau_{res}) \cdot I_s(Q, t), \tag{12}$$

where the time-domain resolution function R(t, $\tau_{res} = 1/\Delta\omega$) plays the role of a cutoff in Eq. (12) beyond $\tau_{res}$. The symmetric elastic scattering function, corrected for detailed balance, is then given by

$$S_R(Q, \omega = 0, \Delta\omega) = \frac{1}{\pi} \int_0^{\infty} dt \cdot I_s(Q, t/\tau_c) \cdot R(t/\tau_{res}). \tag{13}$$

After a change of variables in Eq. (13), one can write the elastic scattering intensity in terms of a scaling function $F_R(x) = F_R(\tau_{res}/\tau_c)$ according to

$$S_R(Q, \tau_{res}, \tau_c) = \tau_{res} \cdot F_R\left(Q, \frac{\tau_{res}}{\tau_c}\right). \tag{14}$$

To explore the ERS function $F_R(Q, \tau_{res}/\tau_c(T))$, one can thus either vary $\tau_{res}$ or the temperature dependent correlation time $\tau_c(T)$. A closely related scaling condition for

temperature scans, ensuring that $\tau_{res}$ and $\tau_c$ are the only relevant time scales, was proposed by Wuttke.[41]

In a typical experiment, one normalizes the elastic scattering function by its value at Q = 0 or by the elastic scattering intensity of the same sample, recorded at a sufficiently low temperature, where quasi-elastic scattering is negligible, thus, $I_s(Q, t = \tau_c(T)) \equiv 1$. The measured spectrum is then identical with the instrumental resolution function. The resulting normalizing elastic intensity is given by the integral of the resolution function in the time domain

$$S_R^0(Q, 0, \Delta\omega) = \frac{1}{\pi}\int_0^\infty dt\, R(t, \tau_{res} = 1/\Delta\omega, \theta). \quad (15)$$

In practice, the resolution function can depend on the scattering angle $\theta$.

The elastic intensity $S_R(Q,0)$ is then interpreted in terms of the average observation time $\langle\tau_{res}\rangle$ defined by

$$\langle\tau_{res}\rangle = \int_0^\infty R(\tau_{res}, t)\, dt = \pi \cdot S_R^0(\omega = 0, \Delta\omega). \quad (16)$$

Analogously, the integrated time-dependent part F(t) of the intermediate scattering function yields the average relaxation time of the respective process

$$\langle\tau_c\rangle = \int_0^\infty F(t)dt = \pi \cdot S_{qel}(\omega = 0). \quad (17)$$

$S_{qel}(\omega = 0)$ denotes the elastic intensity contributed by the quasi-elastic spectrum of a molecular process F(t) with $F(t\to\infty) = 0$. For a liquid in the "hydrodynamic regime," one has: $S_{qel}(Q, 0) = 1/(\pi D_s Q^2)$, where $D_s$ denotes the self-diffusion coefficient of the liquid. Note that in this case the extrapolation of the elastic intensity to zero Q diverges. The elastic intensity thus reflects a "dynamic" property, since it varies between the average resolution time $\langle\tau_{res}\rangle$ at low resolution and the average correlation time of the molecular process $\langle\tau_c\rangle$ at high resolution. Equations (16) and (17) assign a precise meaning to average correlation times including non-exponential relaxation functions. The relevant experimental quantity is a properly normalized elastic intensity $I_{el}^N(Q, \tau_{res})$ combining Eqs. (14) and (15)

$$I_{el}^N(Q, \tau_{res}) = S_R(Q, 0, \Delta\omega)/S_R^0(Q, 0, \Delta\omega). \quad (18)$$

The central idea of ERS is then to derive the approximate intermediate scattering function $I_s(Q, t = \tau_{res}(T))$ from the properly corrected elastic intensity versus the resolution time

$$I_s(Q, t = \tau_{res}) = REISF(Q, \tau_{res}) \approx I_{el}^N(Q, \tau_{res}). \quad (19)$$

The $REISF(Q, \tau_{res})$ differs from $I^N{}_{el}(Q, \tau_{res})$, since the latter includes a quasi-elastic intensity at $\omega = 0$, while the former only records the true elastic intensity. This difference, usually ignored in elastic scattering studies, will be small only for a small ratios $\tau_{res}/\tau_c$.

### C. The Lorentz-Lorentz (LL) model

We first consider the simple case of a double exponential decay and thus Lorentzian spectra for both, resolution- and relaxation function. The integrand on the right hand side of

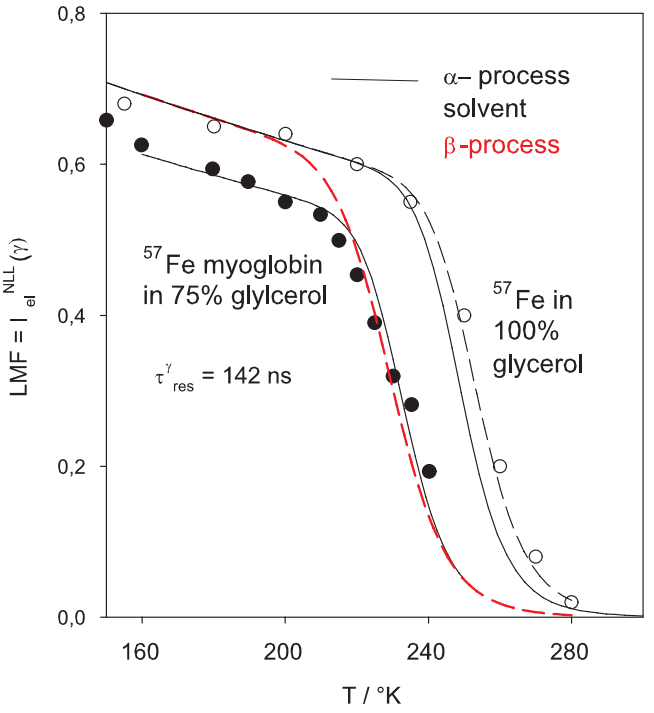


FIG. 3. Lamb-Mössbauer factor of $^{57}$Fe in 100% glycerol[42] and myoglobin in 75% glycerol water[45] and simulations according to the Lorentz-Lorentz model of Eq. (20b): $\tau_{res} = 142$ ns, EISF = 0, $\tau_c(T)$ for $\alpha$-relaxation[19,46] and $\beta$-relaxation (red).[19] The rates of the perfect fit, dashed line, differ by less than a factor of two from the bulk $\alpha$-relaxation rates.[46]

Eq. (13) then has the following form:

$$I_R(Q, t) = QEISF(Q) \cdot \exp\left(-\frac{t}{\tau_c}\right) \cdot \exp\left(-\frac{t}{\tau_{res}}\right) + EISF(Q). \quad (20a)$$

This yields for the normalized elastic intensity $I_{el}^{NLL}(Q)$

$$I_{el}^{NLL}(Q, \tau_{res}, \tau_c) = QEISF(Q)\frac{1}{1+\tau_{res}/\tau_c(T)} + EISF(Q). \quad (20b)$$

QEISF = 1 − EISF and $\tau_{res}^{-1} = \Delta\omega$ denotes the half-width of the Lorentzian resolution function. A useful application of the LL model is the Mössbauer effect. Elastic Mössbauer resonance absorption spectra of $^{57}$Fe are often cited in the context of neutron elastic scattering and the PDT.[42–44] Here, $\tau_{res} = \tau_N = 142$ ns, denotes the nuclear lifetime of the $^{57}$Fe nucleus. Fig. 3 displays the Lamb-Mössbauer factor (LMF) of $^{57}$Fe in 100% glycerol (ferro-cyanide) and of myoglobin in 75% glycerol. For $\tau_c(T)$ in Eq. (20b), we insert the Vogel-Fulcher (VFT) fits of the $\alpha$-relaxation of 75% glycerol[45] and of 100% glycerol.[19,46] The only fit parameter required is the temperature coefficient of the vibrational displacements of the Debye-Waller factor ($2.3 \times 10^{-3}$/K). The LMF is well reproduced by the $\alpha$-process of the solvent: For $^{57}$Fe in 100% glycerol, the rate is only slightly smaller than the bulk rate. The secondary ($\beta$) relaxation, however, taken from Ref. 19 (Fig. 1), does not reproduce the LMF-data of 100% glycerol. This example shows that from elastic scans

alone one can derive the relevant dynamic information, if the assumptions are justified. However, this kind of resolution-dependent analysis was never applied to proteins in this field. It was assumed instead that the drop in elastic intensity implies a true increase in motional amplitudes.[43] The topic of temperature dependent elastic scans will be treated in greater detail in Sec. III D. For small values of $\tau_{res} \ll \tau_c$, one can expand Eq. (20b) to give

$$I_{el}^{NLL}(Q, \tau_{res}) \approx QEISF(Q) \cdot (1 - \tau_{res}/\tau_c) + EISF(Q) \approx QEISF(Q) \cdot \exp(-\tau_{res}/\tau_c) + EISF(Q). \quad (21)$$

For n multiple exponential processes ($\tau_{ci}$), one has in the limit of $\tau_{res} \gg \tau_{ci}$

$$I_{el}^{NLL} \approx EISF(Q) + QEISF(Q) \cdot \langle \tau_c \rangle / \tau_{res} \quad (22)$$

with $\langle \tau_c \rangle = 1/n\ \Sigma\tau_i$, the average correlation time of resolved multiple processes, if $\tau_{res}$ is sufficiently large. From the step-like decrease of the elastic intensity above a certain temperature, one can define a cross-over temperature $T_d$ by $\tau_{res} = \tau_c$ where the elastic intensity due to this process is reduced by a factor of two. If the temperature-dependent relaxation time can be approximated by $\tau_c(T) = \tau_0 \exp(\Delta H^*/RT)$, one obtains from $\tau_{res} = \tau_c\ (T_d)$[25]

$$\Delta H^* = RT_d \ln\left(\frac{\tau_{res}}{\tau_0}\right) \quad (23)$$

and from Eq. (20b) one has the interesting relation for the slope at $T_d$

$$\frac{d}{dT} I_{el}^{NLL}(Q, T_d) = \frac{1}{2}\frac{\Delta H^*}{RT_d^2} QEISF(Q). \quad (24)$$

Equations (23) and (24) yield the activation energy $\Delta H^*$ and the pre-exponential $\tau_0$ if QEISF(Q), as a consistency check, is determined from the data at different Q values.

### D. The δ-correlated resolution function and T-dependent ERS

Since the ERS scaling function $F_R(Q, \tau_{res}/\tau_c)$ (Eq. (14)) depends only on the ratio $\tau_{res}/\tau_c$, one can derive the respective dynamic information at fixed resolution, by varying $\tau_c(T,\eta_s)$ with temperature and solvent viscosity $\eta$.[24,25] Following Ref. 24, we discuss the special case of a $\delta$-resolution function, $R(t, \tau_{res}) = \delta(t - \tau_{res})$, where the difference between elastic fraction and elastic intensity vanishes. It can be used to simulate real experiments with Gaussian resolution functions as shown below. The corresponding Fourier transform to the frequency domain is then given by

$$R'(\omega) = \frac{1}{\pi}\int_0^\infty \cos(\omega \cdot t) \cdot \delta(t - \tau_{res})dt = \frac{1}{\pi}\cos(\omega \cdot \tau_{res}). \quad (25)$$

If Eq. (25) is inserted into Eqs. (12) and (13), it follows that the elastic intensity, recorded in the frequency domain equals the elastic fraction at $\tau_{res}$

$$S_R(Q, \omega = 0, \Delta\omega)_\delta = \frac{1}{\pi} I_s(Q, \tau_{res}) = \frac{1}{\pi} REISF(Q, \tau_{res}). \quad (26)$$

Recording the elastic intensity at variable instrumental resolution in this case solves the full dynamic problem: one can map out the complete intermediate scattering function in the time domain.

In super-cooled liquids and other complex materials such as proteins, the relaxation function is generally composed of multiple dynamic components. As a model of heterogeneous relaxation, the stretched exponential or Kohlrausch function is frequently applied

$$I_K(Q, t) = (1 - EISF(Q)) \cdot \exp(-t/\tau_c)^\beta + EISF(Q). \quad (27)$$

$\beta \leq 1$ denotes the stretching exponent.

Fig. 4(a) shows the Kohlrausch function on a time scale normalized to the structural relaxation time $\tau_c(T)$. With decreasing $\beta$, the time decay broadens by fast and slow components compared to the mono-exponential case of $\beta = 1$. The relaxation functions coincide independently of the shape of the relaxation time spectrum and $\beta$, at $t/\tau_c = 1$. The average relaxation time is obtained from $\langle \tau_c \rangle = \beta^{-1}\ \Gamma(\beta^{-1})\ \tau_c$. Elastic scattering experiments are often performed using back-scattering at fixed instrumental resolution by varying instead the temperature. Fig. 4(b) shows the resulting temperature-dependent elastic intensity $REISF(\tau_{res}, \tau_c(T))$ from Eqs. (26) and (27).[24]. For the correlation time $\tau_c(T)$, an Arrhenius law with an activation energy of 17 kJ/mol and a pre-factor $\tau_0 \cong 10^{-13}$ s was assumed, which is typical of protein hydration water. $\tau_{res}$ was set to 2 ns typical for back-scattering spectrometers (HFBS, SPHERES, IN16). All curves coincide at the dynamic transition temperature $T_d$ independent of $\beta$ at $REISF(T_d) = 1/e$, while the onset temperatures $T_{on}$, which are commonly used to identify the dynamic transition temperature, vary strongly with the stretching exponent and thus the shape of the relaxation time distribution. This complication is avoided, if the transition temperature is by $T_d$ instead of $T_{on}$, where the elastic intensity has decayed to 1/e of its initial value. The final plateau value, the EISF has to be subtracted.[24] If this step, describing the cross-over from elastic to visco-elastic structural behavior, is solvent-induced, we call it a "dynamical transition"[7,24] in analogy to the glass transition of the bulk solvent.

### E. Gaussian resolution functions and Voigtian spectra

The resolution function of most neutron time of flight- and back-scattering spectrometers is rather well approximated (except the low intensity spectral wings) by a Gaussian. For exponential relaxation, a Lorentzian spectrum convoluted with a Gaussian resolution function is recorded which results in a Voigtian spectral line-shape $V(\omega,\sigma,\gamma)$

$$V(\omega, \sigma, \gamma) = \int_{-\infty}^{\infty} d\omega' G(\omega', \sigma) L(\omega - \omega', \gamma), \quad (28)$$

$$G(\omega, \sigma) = \frac{1}{\sqrt{2\pi}\sigma} \exp(-\omega^2/(2\sigma^2)), \quad (29)$$

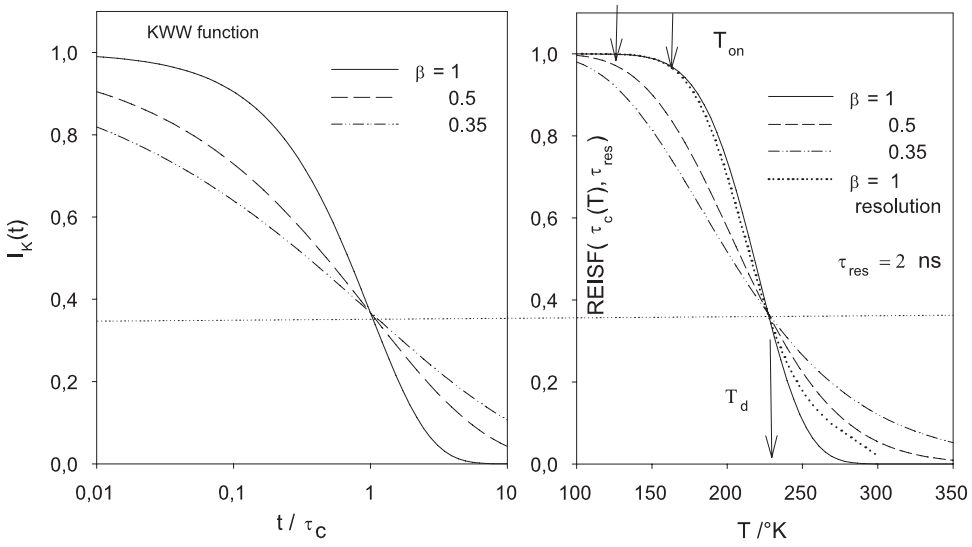


FIG. 4. (a) Kohlrausch intermediate scattering function at different stretching exponents $\beta$ on a reduced time scale, $\tau_c$(T) denotes the temperature structural relaxation time. (b) Resulting elastic intensity according to Eqs. (26) and (27) at fixed resolution time $\tau_{res} = 2$ ns. For $\tau_c$(T), an Arrhenius law was assumed $\tau_0 = 10^{-13}$ s and $H^* = 17$ kJ/mol. The transition temperatures $T_{on}$ and $T_d$ are indicated by arrows. The dotted line illustrates the effect of a Gaussian resolution function for $\beta = 1$.[24]

$$L(\omega, \gamma) = \frac{1}{\pi} \frac{\gamma}{\omega^2 + \gamma^2}, \tag{30}$$

with $\gamma = 1/\tau_c$.

The defining integral (28) can be evaluated in closed form

$$V(\omega, \sigma, \gamma) = \frac{1}{\sqrt{2\pi}\sigma} \mathrm{Re}\{erf(z)\}. \tag{31}$$

Re{erf(z)} denotes the real part of the complex the error function with $z = (\omega + i\gamma)/(\sigma\sqrt{2})$.

Substituting the definition of the complex error function into (31) yields

$$V(z) = \exp(-z^2) \cdot erfc(-iz), \tag{32}$$

where erfc(z) denotes the complementary error function. We are interested in the special case of elastic scattering at $\omega = 0$[30,31]

$$V(\omega = 0, \sigma, \gamma) = \frac{1}{\sqrt{2\pi}\sigma} \exp(\gamma^2/(2\sigma^2) \cdot erfc(\gamma/\sqrt{2}\sigma), \tag{33}$$

which, if inserted into Eq. (18), leads to the following normalized elastic scattering intensity:

$$I_{el}^{NG}(Q, \sigma) = \sqrt{2\pi}\sigma \cdot V(0, \sigma, \gamma) \cdot QEISF(Q) + EISF(Q). \tag{34}$$

With this equation, one can fit experimental data of normalized elastic scattering intensities taken as a function of the instrumental resolution time $\tau_{res}$. Since $\mathrm{erfc}(x) \cdot \exp(x^2) \approx \exp(-x)$ for $x \ll 1$, an exact short time expansion of I(Q, t) is obtained, if we choose the time scale by $t = \tau_{res}$.

TOF and BS spectrometers provide dynamic information in the frequency domain, recording the energy exchange $\Delta E = \hbar\omega$ between neutrons and sample atoms. The width of the resolution function at FWHW is commonly given in energy units, $\Delta E^G_{FWHM}$ [meV]: From Eq. (33), one derives a relation connecting $\tau_{res}$ and $\Delta E^G_{FWHM}$[31]

$$\tau_{res} = 1/(\sqrt{2}\sigma), \tag{35}$$

$$\Delta E^G_{FWHM} = 2\hbar\sqrt{(2\ln 2)}\sigma,$$

$$\tau_{res} = 2\hbar\sqrt{\ln(2)}/\Delta E^G_{FWHM} \approx 1.1\,ps/\Delta E^G_{FWHM}\,[\mathrm{meV}]. \tag{36}$$

Combining Eqs. (35) and (36) yields for the average relaxation time at $T_{on}$

$$\tau_c(T_{on}) \approx 5\tau_{res} = 5.5\,ps/\Delta E^G_{FWHM}\,[\mathrm{meV}]. \tag{37}$$

Fig. 5 shows the relaxation times $\tau_c(T_{on})$ (red open squares) of protein hydration water of lysozyme and c-phycocyanin (CPC) that we have determined based on Table I and experimental onset temperatures (Eq. (37)) assuming exponential relaxation. This is compared to the data for lysozyme of Chen *et al.*[26] (blue) and the RENS results by Magazu *et al.*[16–19] (red squares). Error bars were estimated by accounting for uncertainties in determining $T_{on}$ and the resolution of the spectrometers. The ERS data agree with the RENS results and those of Chen *et al.*[26] at 270 K.

Our $\tau_c(T_{on})$ data, however, show no sign of a dynamic cross-over at 220 K. The same conclusion was obtained in our previous dynamic analysis of D-CPC hydration water. The respective average relaxation times of hydration water

TABLE I. List of instrumental resolution parameters.

| Instrument | ΔE(FWHM) [μeV] | $\tau_{res}$ [ns] | $T_{on}$ [°K] | $\tau_c$ ($T_{on}$) [ns] |
|---|---|---|---|---|
| SPHERES (Munich) | 0.62 | 1.8 | 215 ± 5 | 8.9 |
| HFBS (NIST) | 0.85 | 1.3 | 220 | 6.5 |
| IN10 (Grenoble) | 1.0 | 1.1 | 220 | 5.5 |
| IN13 (Grenoble) | 8.0 | 0.138 | 240 | 0.69 |
| IN6 (Grenoble) | 100 | 0.011 | 270 | 0.015 |

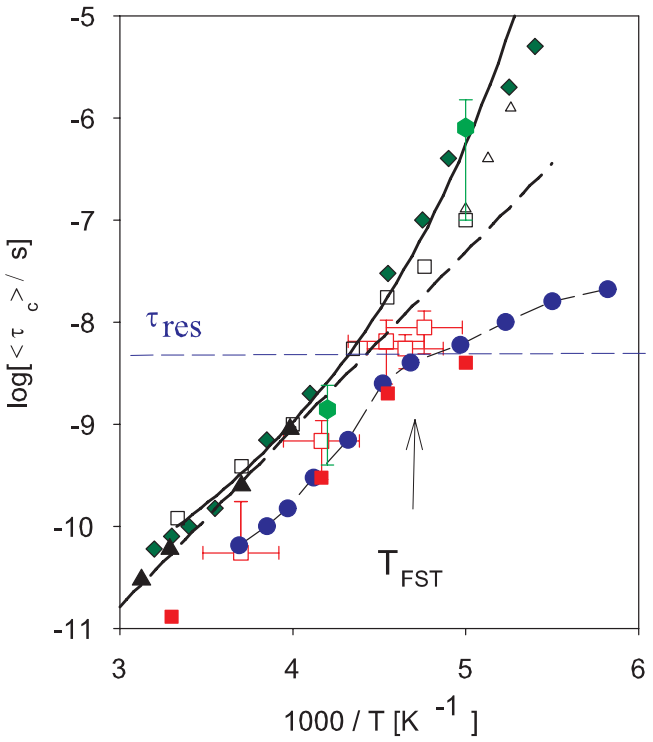


FIG. 5. Arrhenius plot of average hydration water relaxation times: blue circles: hydrated lysozyme (QENS, Chen *et al.*[26]), red squares: lysozyme RENS (Magazu *et al.*[16–18]), open red squares: corrected RENS, lysozyme (this work), open squares: D-PC (QENS, Doster *et al.*[47]), diamonds: D-NMR myoglobin (Vogel *et al.*[48]), open triangles: dielectric relaxation, myoglobin (Swenson and Jansson[49]), full triangles: protein relaxation rate (myoglobin),[47] green hexagons: myoglobin (ERS and Mössbauer effect), dashed line: $\tau_{res}$ instrumental resolution (HFBS) (blue dots). Full line: VFT fit, $H^* = 7(\pm1)$ kJ/mol, $\tau_0 = 6.5(\pm2) \times 10^{-13}$ s, $T_{VFT} = 140(\pm10)$ K, dashed: Arrhenius law, elastic scan of Fig. 7: $\Delta H^* = 17$ kJ/mol, $\tau_0 = 1$ ps, $T_{FST}$: fragile to strong transition temperature.

are shown as open squares in Fig. 5,[47] consistent with D-nuclear magnetic resonance (NMR) results of Vogel *et al.*[48] and with dielectric relaxation data.[49] The lower RENS values result from the assumption of exponential relaxation, the difference would disappear assuming a stretching exponent of $\beta = 0.5$, since $\langle\tau_c\rangle = \tau_c/\beta$. More detailed comments on the RENS approach were published by Wuttke.[41]

### F. The ERS-Gauss approximation of the intermediate scattering function

The ERS function (Eqs. (33) and (34)) approximates the intermediate scattering $I_s(Q, \tau_{res})$ at short times ($\tau_{res} \le \tau_c$) rather well. However, the long-time decay follows a power law $\sim(\tau_{res}/\tau_c)^{-1}$, $\tau_c \gg \tau_{res}$. The origin of this discrepancy is the dominating contribution of the fully resolved quasi-elastic spectrum at zero frequency.[31] With the ERS-TOF method, it is however easily corrected for, since generally complete (noisy) spectra are recorded: The quasi-elastic intensity of the spectrum outside the central elastic line at the non-zero frequency $\omega = \pi\sigma$ is subtracted from the elastic signal at $\omega = 0$. Instead of Eqs. (28) and (31), one considers the corrected Voigtian

$$V_c(\sigma,\gamma) = V(\omega = 0,\sigma,\gamma) - V(\omega = \pi,\sigma,\gamma). \quad (38)$$

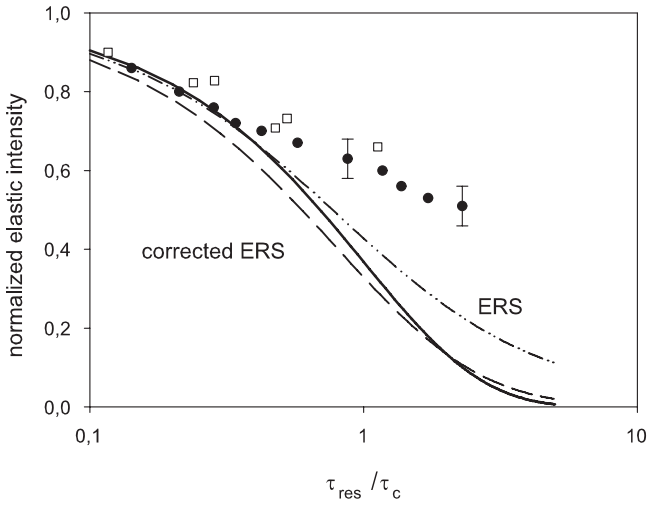


FIG. 6. ERS correlation functions calculated as integral transforms (Eqs. (28) and (29)) of a Lorentzian spectrum using the following $G(\omega)$ kernels. Full line: Fourier kernel, exponential function, dashed-dotted: Gaussian kernel (Eq. (33)), ERS function, dashed line: modified Gauss-kernel, RG: corrected ERS function according to Eq. (40). Black dots: ERS data of hydrated myoglobin (rescaled by a factor 20) and (open squares) alanine dipeptide.[31]

In mathematical terms, the subtraction of the Gauss-convoluted spectrum at finite frequency from the elastic line simulates a Fourier-like resolution function in Eq. (25) with $R_G(\omega,\sigma) \approx \cos(\omega/\sigma)$[31]

$$I^G_{el}(Q,\sigma,\gamma) \propto \int_{-\infty}^{\infty} d\omega \cdot R_G(\omega,\sigma) S(Q,\omega,\gamma) \approx \int_{-\infty}^{\infty} d\omega \cdot \cos(\omega/\sigma) S(Q,\omega,\gamma), \quad (39)$$

which yields with Eqs. (25) and (26)

$$R_G(\omega,\sigma) = G(\omega,\sigma) - 0.5G(\omega-\pi,\sigma) - 0.5G(\omega+\pi,\sigma). \quad (40)$$

$R_G$ approximates the Fourier kernel $\cos(\omega/\sigma)$ quite well in the central frequency range as shown in Ref. 31.

Fig. 6 compares an exponential intermediate scattering function $I_s(t)$ with the ERS function of Eq. (34) (EISF = 0). The approximation works well at short times.

Also shown is the corrected ERS function based on Eqs. (38)–(40), which yields a reasonable approximation of $I_s(t)$ particularly at long times. Also shown are rescaled experimental data on hydrated myoglobin and alanine dipeptide. The exponential model approximates the data at short times only due to a finite EISF(Q). The comparison illustrates that the differences between the intermediate scattering function and its ERS approximation are within the experimental noise. The Fourier-like kernel and the $\delta$-correlated resolution function, which was assumed in Sec. III D, are well approximated experimentally with $R_G$ of Eq. (40).

## IV. DISCUSSION OF EXPERIMENTAL RESULTS

### A. Activation parameters and relaxation time spectra from back-scattering ERS

In Sec. III C and Fig. 3, it was shown how to determine the activation parameters from elastic temperature scans

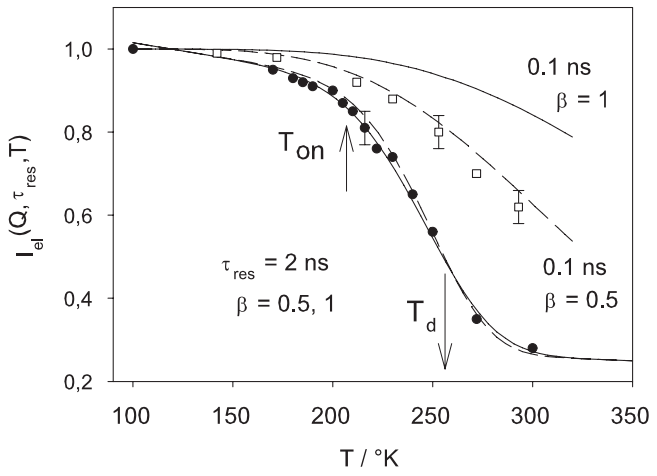


FIG. 7. Elastic scans of protein hydration water at Q = 1 Å$^{-1}$: full circles: C-PC with 0.3 g/g $H_2O$ (full circles) at a resolution of $\tau_{res} \approx 2$ ns (SPHERES), normalized at $T_0 = 100$ K, open squares: $H_2O$-hydrated myoglobin at a resolution of 0.1 ns (IN13), lines: fits to the stretched exponential model of Eq. (27) including a vibrational Debye Waller factor at $\beta = 0.5$ (full line) and 1.0 (dashed). The temperatures $T_{on}$ and $T_d$ are indicated by arrows. The parameters are given in the text.

at fixed resolution. In this section, we investigate the effect of performing such experiments at different instrumental resolution. Table I lists the resolution parameters of several back-scattering spectrometers. The respective resolution times cover a narrow range near 1 ns. To expand the time window, one includes TOF instruments or varies the temperature instead.

Fig. 7 illustrates how this concept of temperature-dependent elastic scans is applied to study the dynamics of protein hydration water, $H_2O$-hydrated per-deuterated phycocyanin (C-PC).[24,47] The per-deuteration of the protein emphasizes the scattering fraction of protein hydration water. The resolution time of the back-scattering spectrometer SPHERES (JNCS, FRM2) was approximately $\tau_{res} \approx 2$ ns.

The elastic scattering intensity was normalized to its value at 100 K. The decrease in elastic intensity between 100 and 200 K is determined by the vibrational Debye–Waller factor of the protein-water system. The extra loss above the onset temperature $T_{on} \approx 220$ K can be attributed to an increasing resolution of the diffusional motions of hydration water.[40,47] The genuine elastic scattering, ≈0.25 estimated from the high temperature plateau and spin polarized elastic scattering experiments,[33] is dominated by the powder averaged coherent structure factor $S_{coh}(Q)$ of the protein structure. For mobile $H_2O$, one expects EISF(Q) = 0. After corrections for S(Q) and the vibrational component, one derives from the 1/e value of the elastic intensity $T_d \approx 255$ K. At this temperature, the correlation time of hydration water $\tau_c$ coincides with $\tau_{res} \approx 2$ ns. This agrees quite well with the result of the full spectral analysis in Fig. 5.[47] For a precise definition of $T_d$, the complete transition curve is required and not just the onset, in particular the plateau at high temperatures needs to be established. Instead of focussing on a single temperature, in practice one performs fits of the complete PDT transition curve. For the narrow range of the transition, we assume an Arrhenius law for the average correlation time: $\tau_c = \tau_0 \cdot \exp(\Delta H^*/RT)$. The curves shown in Fig. 7 refer to two values of the stretching exponent: $\beta = 1$ (long dashed) yields the activation energy of 17 kJ/mol and a pre-exponential of $10^{-13}$ s. The full line, $\beta = 0.5$, yields an activation energy of $\Delta H^* = 33$ kJ/mol (dashed 35 kJ/mol, to show the sensitivity) and a pre-exponential of $\tau_0 = 10^{-15}$ s. Fig. 5 compares the Arrhenius plot of $\langle \tau_c \rangle$ derived from the elastic scan (dashed line) with values deduced from of a full dynamic analysis. The Arrhenius law approximates the data quite well in the vicinity of $\tau_{res} \cong \tau_c$ in the temperature range $T_{on}$, $T_d$.

Using the above stretched exponential model and an Arrhenius law to get identical elastic intensities $I_{el}(T)$ for $\beta < 1$ with respect to $\beta = 1$, the following condition has to be obeyed:

$$\exp(-\tau_{res}/\tau_c(T)) = \exp\left(-\left(\tau_{res}/\tau_c^{\beta}(T)\right)^{\beta}\right). \tag{41a}$$

For the respective activation energies, this implies

$$\Delta H_{\beta}^* = \Delta H_1^*/\beta, \tag{41b}$$

for the pre-exponential, one has

$$\tau_{01}(T) = (\tau_{res})^{1-\beta}\, \tau_{0\beta}^{\beta} \tag{41c}$$

to yield the same elastic scan $I_{el}(\tau_{res}, T)$. Equation (41c) describes the relation between the fitted pre-exponentials for $\beta = 1$ and $\beta < 1$, which depends on the resolution time $\tau_{res}$.

Thus, fitting elastic scans performed at different instrumental resolution opens the possibility to get an estimate of the stretching exponent $\beta$: The pre-exponential will be independent of the resolution time only for the correct $\beta$-value, assumed to be temperature independent.

Fig. 7 also shows an elastic scan of myoglobin hydration water performed at a resolution of 140 ps. Using the parameters derived for CPC hydration water at a different resolution leads to a reasonable fit of the data only for $\beta = 0.5$. The predicted curve for $\beta = 1$ cannot account for the data.

The value of $\beta$ cannot be deduced from elastic scan experiments performed at a single resolution. The width parameter and the activation parameters are then degenerate. Multiple scans performed at several instrumental resolution times can solve the problem.

In conclusion, the temperature dependent ERS analysis with back-scattering instruments, if properly performed, can yield the full dynamic information comparable to quasi-elastic scattering: (1) temperature dependent average relaxation time including pre-exponential and activation energy of the Arrhenius law, (2) the width parameter of the relaxation time spectrum, (3) the EISF and the vibrational Debye-Waller factor, (4) to achieve the same information using QENS much more beam time would be required, since at each temperature a high-quality quasi-elastic spectrum would have to be recorded.

The main assumption behind the temperature-dependent ERS analysis is the time-temperature superposition principle requiring a molecular mechanism, which is continuous with the temperature.

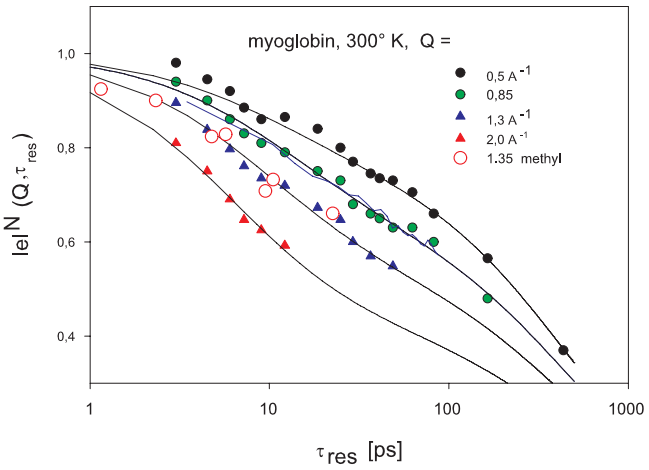


FIG. 8. ERS elastic intensity, $I_{el}^{N}(Q, \tau_{res})$ of $D_2O$-hydrated myoglobin, (h ($D_2O$) = 0.35 g/g protein, $m_{Mb}$ = 25 mg) normalized to data at 150 K at different Q, (IN 5 Grenoble) versus reciprocal Gaussian line-width of the resolution function, $\tau_{res} = 2\hbar/\sigma_E$. Full lines: two-exponential Voigtian fit according to Eq. (34). For comparison, ERS data with alanine-dipeptide (open circles, NEAT, Berlin) of Fig. 10 are displayed, which reflect the methyl group rotation of the side chain.[21,22]

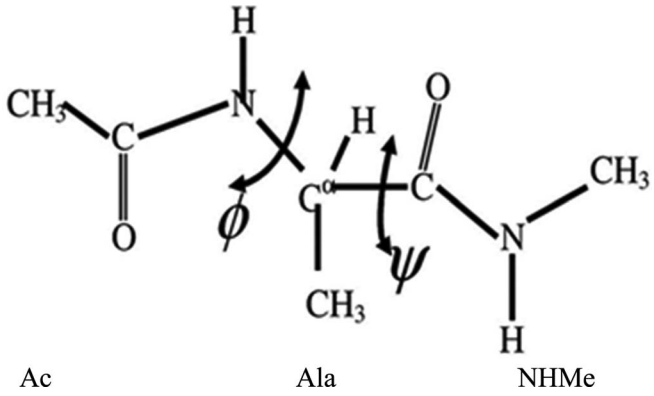


FIG. 9. Chemical structure of the alanine dipeptide with the flexible backbone dihedral angles $\phi$, $\psi$ as indicated. We label the C-terminal blocking group, Ac, the alanine residue as Ala, and the N-terminal blocking group as NHMe.

## B. The protein dynamical transition at room temperature from TOF-ERS

In contrast to back-scattering spectroscopy, where the resolution is essentially fixed, TOF spectroscopy can cover a wide range from $\tau_{res} \approx 1$ ps to several hundred ps. The Gaussian energy resolution (FWHM) of the TOF spectrometer IN5 can be calculated from $\Delta E_G = 273\,400/(\lambda_i^3 \cdot S)$ [meV Å$^3$ rpm]. The energy width decreases strongly with increasing incident wavelength, however, in parallel the flux and the accessible Q-range decrease. Since only the elastic intensity is of interest, one can further increase the signal by running the chopper, which prevents frame-overlap, in phase with the frame setting choppers (ratio 1 instead of 2 or 3). When the frame overlap becomes significant even in the elastic region (> 10 000 rpm), it is possible to correct for it.[31] The restriction to the elastic region makes it feasible to use long wavelengths and high chopper speeds, which would be impractical for conventional QENS. Table II of the supplementary material[57] shows a possible ERS setup with the corresponding parameters of flux, Q-range, and energy resolution for IN5. This setup can be used for nearly all TOF spectrometers. In the first ERS experiment at IN5 with 25 mg of $D_2O$-hydrated myoglobin,[30] the chopper speed was varied between 1000 and 20 000 rpm. Wavelength of 5, 8, 12, 16 Å were chosen. The corresponding energy resolution varied from 5 to 500 $\mu$eV, covering about 2 decades. The data reveal two time- and Q- dependent processes covering two and a half decades. The fast process could be assigned to methyl rotation, the second process is assigned to water-coupled libration of side chains (Fig. 8). The ERS method thus provided the first assignment of a spectral component to methyl group rotation in proteins at room temperature.[30,31] Instead of observing the "onset" of methyl rotation at 100 K,[50] one can study the respective dynamics at physiological temperatures. This applies in particular to the solvent induced elastic decrease versus resolution, the high temperature PDT. A full elastic analysis of methyl group rotation in myoglobin was published in 2005.[2]

## C. ERS-TOF analysis of alanine dipeptide (ADP)

### *1. Alanine dipeptide (N-methyl-L-alanyl-N-methylamide)*

$CH_3$–CONH–$C_\alpha H(C_\beta H_3)$–CONH–$CH_3$ is one of the simplest model peptides and serves as a paradigm to theoretical studies.[51] Its chemical structure is displayed in Fig. 9. This peptide contains many structural features, which are typical of a protein backbone: flexible dihedral angles ($\varphi$ and $\psi$), the presence of multiple CO and NH units for H-bonding and a pendant side chain methyl group. The N- and C-terminal groups have low rotational barriers (~3 kJ/mol) and perform diffusive motions on pico-second time scale. The barrier for the side-chain methyl group is larger (~7.5 kJ/mol). In Fig. 1, the conventional quasi-elastic spectrum of alanine dipeptide crystal is displayed, observed with the TOF spectrometer NEAT at BENSC (Berlin). The data illustrate the problem of observing two processes with very different correlation times simultaneously using a single instrumental resolution. In the present case, a compromising relatively high resolution of 47 $\mu$eV (FWHM) was chosen. Ideally, one should have performed two quasi-elastic experiments at 20 and 100 $\mu$eV to characterize the two processes accurately. This requires merging spectra derived at different instrumental conditions. Instead of choosing two resolutions, one could vary the resolution continuously within a wide range and save beam time by focusing on the elastic intensity as discussed above. In the particular case of alanine dipeptide, the chopper speed was varied between 1000 and 10 000 rpm at three wavelengths 5, 8, and 10 Å. A maximum of 20 000 rpm can be achieved. This procedure required about 12 h of beam time for 300 mg of sample including vanadium standard experiments. The ERS function (uncorrected) is shown for three Q-values in Fig. 10. From the scattering cross-section, one can predict the EISF(Q) for the three methyl groups. The dashed line reflects the ERS prediction due to rotational transitions of three methyl groups. The analysis shows that both, the

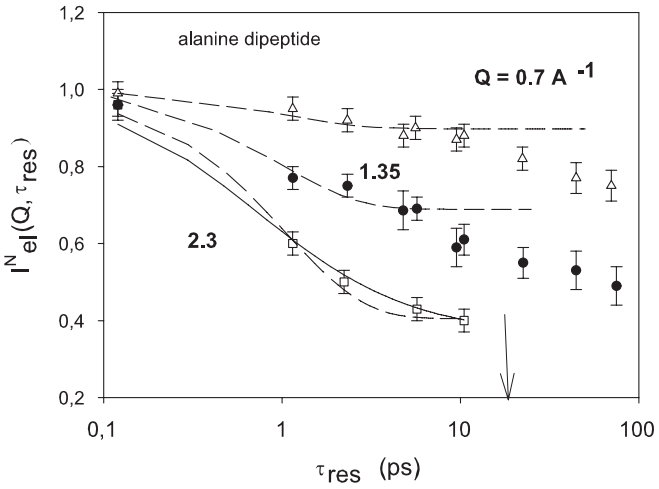


FIG. 10. ERS intermediate scattering function of alanine dipeptide at 300 K versus the TOF resolution time (NEAT, BENSC Berlin) at various Q.[22] The dashed lines represent the combined correlation function of the three methyl groups accounting for the appropriate cross-sections. The full line at Q = 1.35 Å$^{-1}$ denotes the Fourier transform of the QENS result of Fig. 1, the arrow indicates the QENS resolution time. The full line at Q = 2.3 Å$^{-1}$ implies exponential relaxation in comparison with the ERS function (dashed). Adapted from Ref. 31.

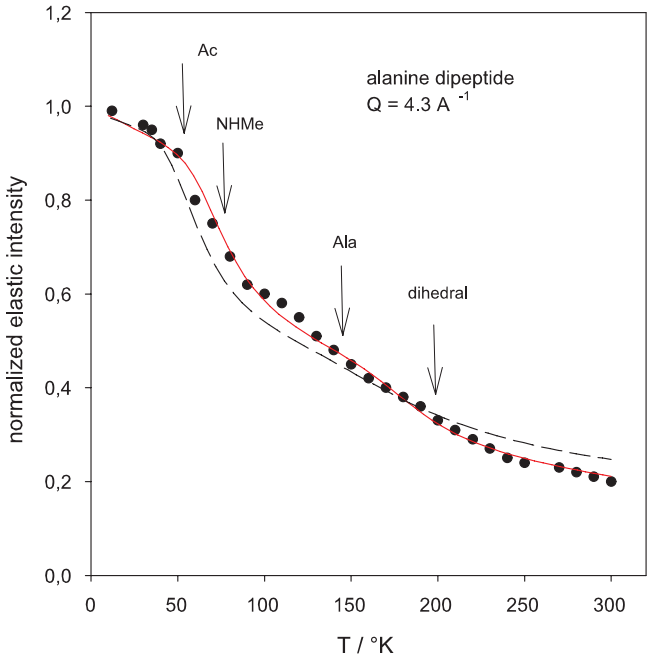


FIG. 11. Normalized elastic scattering intensity $I_{el}^{NG}(Q = 4.3$ Å$^{-1}$, $\tau t_{res} = 137$ ps) of alanine dipeptide crystal powder (back-scattering spectrometer IN13, ILL, Grenoble) and a 4-component fit (Eq. (34), red line) accounting for the fast C-(Ac) and N-(NHMe) terminal blocking methyl groups ($T_{on} \cong 50$ K), the side chain methyl(Ala) ($T_{on} \cong 150$ K), and the dihedral transitions ($T_{on} \cong 210$ K). To show the sensitivity of the fit, the dashed line accounts for Ac and the Ala methyls only. The arrows indicate the location of the respective $T_{on}$ values.

terminal and the side chain methyl groups, rotate on a picosecond time scale ∼2 ps at 300 K. The full line at Q = 1.35 Å displays the Fourier transform of the fit of the quasi-elastic spectrum shown in Fig. 1. The frequency and the time domain data agree reasonably well, however, the ERS function decays further at long times below the value predicted for fully resolved rotational transitions. Thus, a second process with a characteristic time of 20 (±3) ps must exist, which is partially resolved in the QENS data as a narrow line in Fig. 1. This result suggests a reorientation of the methyl group rotational axis due to dihedral angle transitions. In model calculations, we obtain rather large angular changes ∼40°. For comparison of the two methods, we also perform a temperature dependent elastic scans of ADP at fixed resolution (∼140 ps) shown in Fig. 11. The elastic scattering function at the particular Q-value was calculated based on the cross-sections and partial scattering functions of the three methyl groups (Eq. (2)). Four dynamic components are required to account for the data. The dashed line with only two dynamic components does not agree with the data. The respective onset temperatures $T_{on}$ are indicated by arrows.

The analysis shows that the C- and N-terminal methyl groups of ADP ($T_{on} \cong 50$ K) are not equivalent as was assumed in early MD simulations.[51] The rotational transition times are deduced from an Arrhenius law according to $\tau_c = \tau_0 \exp(\Delta H^*/RT)$. This yields for the terminal groups $T_{on} \cong 50$ K, $\Delta H^* = 2.5$ and 4.2 (±0.2) kJ/mol with a common pre-exponential $\tau_0 = 0.1$ ps. For the side chain, we fit $T_{on} \cong 150$ K, $\Delta H^* = 9.1$ (±2) kJ/mol. The structural relaxation process with $T_{on} \cong 200$ K yields $\Delta H^* = 14$ (±1) kJ/mol. The temperature coefficient of the vibrational Debye Waller factor is 0.0014 Å$^{-2}$/K at Q = 4.2 Å$^{-1}$. The vibrational mean squared displacement of ADP crystals at 300 K then amounts to $\langle \Delta x^2 \rangle_{vib} = 0.024$ (±0.002) Å$^2$. Onset temperatures in the range of 50-100 K are typical of acetyl methyl groups. Such side chains do not occur in proteins but sometimes in buffers: acetate is often contained in commercial protein preparations and needs to be carefully removed from sample preparations. For protein methyl side chains, we determined the average activation energy of 10 (±2) kJ/mol[55] slightly larger than the dipeptide side chain. Most interesting is the new structural relaxation process, which is assigned tentatively to transitions of the dihedral angles as the only remaining flexible part of the molecule.

### D. Elastic intensity and mean square displacements (MSD)

A common practice of the EINS method is to determine atomic mean square displacements from the Q-dependence of the elastic intensity. The displacements then carry the time tag of the instrumental resolution.[1–4] The correct method is to evaluate the EISF(Q) and Eq. (3) and not just as usual the elastic intensity. Expanding the isotropic EISF(Q) in the low Q-limit yields the long time MSD[2]

$$EISF(Q \to 0) = 1 - \frac{1}{3} Q^2 \langle \Delta r^2 \rangle_{\omega=0} + O(Q^4). \qquad (42)$$

The time resolved MSD by contrast follows from the low Q expansion of the intermediate scattering function of Eq. (5)[2]

$$I_s(\vec{Q}, t) = 1 - \frac{1}{2} \int d^3\vec{r} (\vec{Q}\vec{r})^2 G(\vec{r}, t) + O\left(\vec{Q}^4\right). \qquad (43)$$

Performing the isotropic average and keeping only terms up to $Q^2$ yields

$$I_s(Q,t) = 1 - \frac{1}{2}\frac{Q^2}{3}\langle r^2(t)\rangle + O(Q^4). \quad (44)$$

The MSDs derived in the time domain at long times, Eq. (44), thus differ from those determined in the frequency domain by a factor of two

$$2\langle \Delta r^2\rangle_{\omega=0} = \langle r^2(t\to\infty)\rangle. \quad (45)$$

The displacements in the time domain $\langle r^2(t\to\infty)\rangle$ reflect the full width at half maximum of EISF(Q), while the "elastic" displacements $\langle \Delta r^2\rangle_{\omega=0}$ are determined experimentally from the half width of EISF(Q) for positive Q-values. In addition, one has $\langle \Delta r^2\rangle_{\omega=0} = 3\ \langle \Delta x^2\rangle_{\omega=0}$ in the isotropic case. The pre-factor is thus not a matter of convention, as often assumed.

In the low Q-limit, the displacement distribution is Gaussian for localized processes, which yields for the elastic fraction (Eq. (10a))

$$REISF(Q,\tau_{res},T)_{Q\to 0} = \exp\left\{-\frac{1}{3}Q^2\langle r^2(\tau_{res},T)\rangle\right\}. \quad (46)$$

For exponential relaxation, one obtains from Eq. (46)

$$\langle r^2(\tau_{res})\rangle_{Q\to 0} \cong \left\langle r_\infty^2\right\rangle \cdot (1-\exp(-\tau_{res}/\tau_c)), \quad (47)$$

where $\langle r^2{}_\infty\rangle$ denotes the displacement at infinite time. Time-resolved displacements of protein hydration water were first published in 1996.[2,40] It is common practice to approximate the elastic fraction by the elastic intensity. The latter is used to determine displacements ignoring the quasi-elastic contribution at $\omega = 0$. This approximation is valid only for the initial decay (onset region) of the elastic intensity implying, $\tau_{res}/\tau_c < 1$. Then Eqs. (46) and (47) can be expanded to give in the low Q-limit

$$I_{el}^N(Q\to 0, \tau_{res}\le\tau_c) \approx 1 - Q^2\left\langle r_\infty^2\right\rangle\cdot\tau_{res}/\tau_c. \quad (48)$$

Equation (48) could be interpreted as the hydrodynamic limit, where the squared displacements increase linearly with time up to the final long time value.

Experimentally, one determines the approximate 1D-displacements in the frequency domain from the slope of the elastic scattering curve extrapolated to low Q values[2,25]

$$\frac{1}{3}\langle \Delta r^2\rangle_{\omega=0} \approx -\frac{\partial \ln I_{el}(Q)}{\partial Q^2} Q\to 0. \quad (49)$$

No pre-factor is involved on the right hand side. In practice, there are complications due to coherent scattering contributions, multiple scattering, deviations from Gaussian behavior, and instrumental artifacts rising at low Q.[52] Due to these problems, the MSD values determined by different authors are sometimes incompatible.

By contrast, our method relies on the Q-dependent elastic intensity, which does not require an extrapolation to low Q.

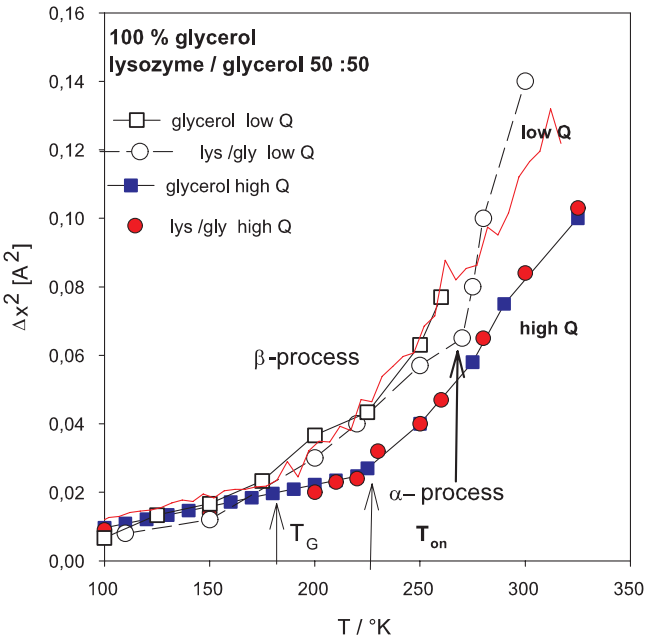


FIG. 12. Apparent 1D mean square displacements of 100% glycerol and lysozyme in glycerol 50:50 at high Q: blue squares: glycerol,[53] red circles: lysozyme/glycerol,[19] and at low Q: open squares: partially deuterated glycerol,[54] open circles: lysozyme/glycerol 50:50,[11] red line: myoglobin total MSD of Fig. 13.

### E. Qualitative MSD analysis: Solvent slaving of lysozyme in glycerol

Most publications in this field focus on MSD plots versus temperature and the determination of $T_{on.}$ A recent example by Capaccioli *et al.*[19] is reproduced in Fig. 12. It compares temperature dependent MSDs of partially deuterated glycerol with those derived from a 50:50 mixture of lysozyme and per-deuterated glycerol (red circles and blue squares). The MSD values of both, bulk solvent and protein solution, superimpose perfectly across the entire temperature range, suggesting that protein structural fluctuations are "slaved" by bulk solvent. This is quite remarkable since the mobility of these molecules is quite different: glycerol is a highly mobile liquid above the glass temperature $T_g$ and can perform long range diffusion, while protein residues are confined by covalent bonds. The apparent displacements of glycerol thus increase with decreasing wave vector Q in contrast to those of localized protein side chains. Reference 19 does not reveal, how the MSD values in Fig. 12 were actually generated. It is however unlikely that the MSDs of lysozyme/glycerol represent Q-values below 1 $Å^{-1}$ according to Eq. (49), since the superimposing MSDs of partially deuterated glycerol by Wuttke *et al.*,[53] were derived from the instrument IN13 at much higher Q ≈ 3-5 $Å^{-1}$. Otherwise, this should lead to diverging results, since the elastic scattering functions are not Gaussian within the entire Q-range. Moreover, glycerol is a liquid, which does not exhibit genuine elastic scattering: The Gaussian approximation is thus neither valid at high nor at low Q-values. This suggests that both MSDs were determined in the same (high) Q-range and reflect the same type of motions. A different MSD set of the same lysozyme-glycerol sample, determined at low Q (below 1 $Å^{-1}$), was published by Tsai *et al.*,[11] and is also shown

(open squares) in Fig. 12. Moreover, Fujara *et al.*[54] have determined the respective low-Q MSD values of the same glycerol sample shown by open squares in Fig. 12. The low-Q MSDs of lysozyme and glycerol also superimpose rather well, but differ significantly from those taken at high Q. Fujara *et al.*[54] terminate their evaluation at 260 K, where the $\alpha$-relaxation of the solvent becomes noticeable in the spectrum. Thus, $T_{on}(\alpha) \cong 260$ K at this resolution with $\tau_{res} \sim 100$ ps. The art of qualitative analysis is now to guess a proper onset temperature and to attach a physical meaning to it. Capaccioli *et al.*[19] deduce from their high Q data two onset temperatures around 220 and 270 K. $T_{on}(1)$ is attributed to a primitive relaxation related to the glass transition at $T_g \sim 180$ K and $T_{on}(2)$ is assigned to a resolved secondary ($\beta$) relaxation above 270 K, which they call $T_d$. The $\alpha$-relaxation does not play any role in their concept. This view does not agree with our results of the Mössbauer LMF for glycerol in Fig. 3, which prove the relevance of the main relaxation. Moreover, the low Q-data clearly demonstrate the emergence of motional amplitudes around $T_g \cong 180$ K, which we have previously identified with fast $\beta$-relaxation.[24] $T_{on}(2)$ around 270 K is attributed by us to the $\alpha$-relaxation of the solvent crossing the time window of the spectrometer. This view is compatible with the interpretation of Fujara *et al.*[54] of their EINS data of glycerol. The puzzle, why the two MSDs of protein and solvent superimpose, remains. One should keep in mind the 20% contribution of per-deuterated glycerol to the total cross-section of the 50:50 mixture even if the protein is fully dissolved. Increasing the protein concentration[11] enhances the vibrational MSDs, due to a change in the cross-sections and a larger methyl group contribution of the protein.

### F. Quantitative analysis of protein-solvent displacements: Hydrated myoglobin

Fig. 13 displays the MSD(T) of $D_2O$-hydrated myoglobin at h = 0.35 g/g (red line in Fig. 12).[2,3,25] The linear temperature range, reflecting vibrational motion, extends up to $T_{on} \approx 170$ K. Then the MSD increases more rapidly due to resolved rotational transitions of side chains.[2,7] The second onset, $T_{on}(140\text{ ps}) \approx 240$ K by contrast, depends on the degree of hydration and was thus assigned to water-coupled collective motions, the PDT.[7] The collective displacements due to the water coupled component have been separated from rotational transitions of side chains and are also shown in Fig. 13. For comparison, we also plot the displacements of the heme group in myoglobin crystals, recorded with Mössbauer spectroscopy at $\tau_{res} = 142$ ns.[43] The onset temperature is located at $T_{on}(142\text{ ns}) \approx 200$ K, 40° less than $T_{on}(\tau_{res} = 140\text{ ps})$ derived from neutron scattering. In the literature, the two onsets are taken synonymously as the signature of the PDT irrespective of different time scales and the different probes. That both effects reflect one and the same process has never been demonstrated convincingly. With our elastic scattering analysis one can now elucidate, whether both methods probe the same process of protein-water structural relaxation at different time scales. The mean square displacements are calculated from scans of the elastic intensity assuming a Gaussian scattering law at low Q.

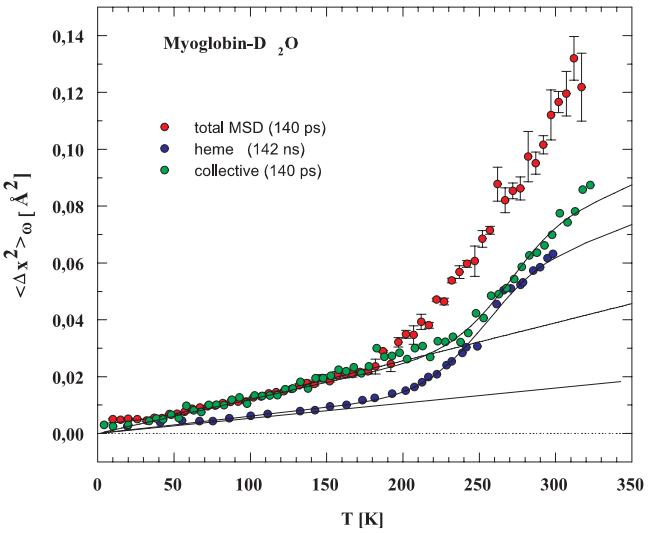


FIG. 13. Mean square displacements of hydrated myoglobin (IN13, ILL), red dots: total displacements (proton), including methyl group rotation, $\tau_{res} \approx 140$ ps, green dots: hydration dependent collective displacements (methyl groups subtracted), blue dots: heme iron of myoglobin (crystals) from Mössbauer LMF, $\tau_{res} = 142$ ns. Lines are fits to a model of a common protein-water relaxation process assuming an Arrhenius law for $\langle\tau_c\rangle$ compatible with the data in Fig. 5: $\Delta H^* \cong 20$ kJ/mol and $\tau_0 \cong 1$ ps.

For $\tau_c(T)$, we insert the average relaxation time of hydration water displayed in Fig. 5. The average relaxation time is sufficient to reproduce the MSDs, no distribution is required. The results, shown in Fig. 13, suggest indeed that both types of displacements, heme group and collective protein fluctuations, couple to motions of the hydration shell on the same time scale.[2,3,25,47] The resulting average correlation times at the respective onset temperatures 240 K and 200 K are 1.4 ns and 2 $\mu$s. These values are plotted in Fig. 5 as green hexagons and fit in very well with those resulting from a spectral analysis of neutron scattering, NMR, and dielectric relaxation. The matching correlation times of protein hydration water and water-coupled protein motions suggest a common mechanism of protein-water visco-elastic relaxation.[2–4] The PDT is thus a special case of the well-known "time-temperature superposition principle," which states that relaxation functions, taken at different temperatures, can be superimposed after renormalization of the structural relaxation time by the solvent viscosity at the particular temperature.[37–39] The relaxation time of hydration water observed with neutron scattering increases with Q as $\tau_c(Q) \sim Q^2$ at low Q, the signature of translational diffusion.[2,3,40] The main structural relaxation is thus dominated above 220 K by $\alpha$-relaxation, local $\beta$-processes would exhibit a Q-independent time constant.

## V. CONCLUSION

The scaling analysis of elastic neutron scattering data, if properly performed, can provide the full dynamic information equivalent to a spectral analysis. A prerequisite is to include the complete elastic scattering function versus temperature, momentum exchange, and instrumental resolution. The ERS method is more powerful than the qualitative RENS approach, where only cross-over temperatures

are considered. The latter is restricted to a narrow temperature range, where structural relaxation time and instrumental resolution time coincide. With back-scattering spectroscopy, temperature-dependent elastic scans at fixed resolution can be performed, while with TOF, the instrumental resolution can be varied by at least two decades. Both methods are equivalent since the dynamic scaling function depends on the ratio of $\tau_{res}/\tau_c(T,\eta,\dots)$. Temperature-dependent scans are quite popular, but the advantage of changing the resolution within a wide range has not been fully explored. The elastic method might be especially useful if only small or per-deuterated biological samples are available or if a wide range of experimental parameters has to be scanned. The ERS thus complements the conventional QENS method without implying a full spectral analysis.

For the model protein, alanine dipeptide, the complete intermediate scattering function based on elastic experiments at fixed temperature was deduced. The terminal and the side-chain methyl groups rotate on a pico-second time scale under conditions of tight packing in the crystal. This suggests that methyl side chains will perform rotational transitions in proteins also on this time scale at room temperature. Even more revealing is the respective temperature dependent elastic scan at fixed resolution. The three methyl groups thus exhibit different rotational barriers in the crystal. Most interesting is a third slow process, assigned to rotational transitions in the dihedral angles, observed with both methods. These results have important implications to understanding protein dynamics and the interpretation of neutron scattering spectra. Elastic scans performed at different instrumental resolution with hydrated proteins yield the activation parameters and the relaxation time spectrum of water coupled motions. The protein dynamical transition is best characterized by a step in the elastic intensity at $T_d$, which is induced by the solvent (Figs. 2, 3, and 7). It specifies the dynamic cross-over from truly elastic to viscoelastic structural behavior ($\alpha$), depending on the probe frequency. The PDT as an elasticity transition should not be confused with the "onset of an-harmonic motions." The an-harmonic onset denotes a precursor of the PDT around $T_g$ specified by an increasing amplitude of fast open-closed hydrogen bond fluctuations above the harmonic level (Fig. 12 at low Q).[2,24] This result differs from those of Capaccioli and Ngai,[19,20] which call the process around $T_g$ "primitive relaxation" and attribute $T_d$ to a local process of the Goldstein-Johari type.

More intense neutron sources will make it possible in the near future, to routinely collect complete inelastic spectra of biomolecules. The "elastic fraction" in addition to the "elastic intensity" is then directly accessible as an important source of dynamic information. But the elastic intensity remains a useful and practical measure of structural displacements, if its limitations are properly understood.


[1] F. Gabel, D. Bicout, U. Lehnert, M. Tehei, M. Weik, and G. Zaccai, Q. Rev. Biophys. **35**, 327 (2002).
[2] W. Doster and M. Settles, Biochim. Biophys. Acta **1749**, 173 (2005).
[3] W. Doster, Biochim. Biophys. Acta **1804**, 3 (2010).
[4] W. Doster and M. Settles, *Hydration Processes in Biology (Les Houches Lectures 1998)*, Nato Science Series A: Life Science Vol. 305 (IOS Press, 1999), p. 177.
[5] W. Doster, in *Neutron Scattering in Biology*, edited by J. Fitter, T. Gutberlet, and J. Katsaras (Springer, 2006), p. 461.
[6] S. Longeville and W. Doster, in *Dynamics of Soft Matter, Neutron Applications*, edited by V. G. Sakai (Springer Science, 2012), Chap. 8.
[7] W. Doster, S. Cusack, and W. Petry, Nature (London) **337**, 754 (1989).
[8] M. Ferrand, A. J. Dianoux, W. Petry, and G. Zaccai, Proc. Natl. Acad. Sci. U.S.A. **90**, 9668 (1993).
[9] J. Fitter, R. E. Lechner, and N. A. Dencher, Biophys. J. **73**, 2126 (1997).
[10] G. Zaccai, Science **288**, 1604 (2000).
[11] A. M. Tsai, D. A. Neumann, and L. Bell, Biophys. J. **79**, 2728 (2000).
[12] V. Reat, R. Dunn, M. Ferrand, J. L. Finney, R. M. Daniel, and J. C. Smith, Proc. Natl. Acad. Sci. U.S.A. **97**, 9961 (2000).
[13] G. Schiro, C. Caronna, F. Natali, and A. Cupane, Phys. Chem. Chem. Phys. **12**, 10215 (2010).
[14] H. Nakagawa, H. Kamikubo, I. Tsukushi, T. Kanaya, and M. Kataoka, J. Phys. Soc. Jpn. **73**, 491 (2004).
[15] A. Paciaroni, E. Cornicchi, A. De Francesco, M. Marconi, and G. Onori, Eur. Biophys. J. **35**, 591 (2006).
[16] S. Magazu, F. Migliardo, and A. Benedetto, J. Phys. Chem. B **114**, 9268 (2010).
[17] S. Magazu, F. Migliardo, and A. Benedetto, J. Phys. Chem. B **115**, 7736 (2011).
[18] S. Magazu, F. Migliardo, and A. Benedetto, Rev. Sci. Instrum. **82**, 105115 (2011).
[19] S. Capaccioli, K. L. Ngai, S. Ancherbak, and A. Paciaroni, J. Phys. Chem. B **116**, 1745 (2012).
[20] K. L. Ngai, S. Capaccioli, and A. Pacciaroni, J. Chem. Phys. **138**, 235102 (2013).
[21] G. Schiro, C. Caronna, F. Natali, M. M. Koza, and A. Cupane, J. Phys. Chem. Lett. **2**, 2275 (2011).
[22] G. Schiro, F. Natali, and A. Cupane, Phys. Rev. Lett. **109**, 128102 (2012).
[23] G. L. Squires, *Introduction to Thermal Neutron Scattering* (Dover Books on Physics, 1996), pp. 73–75.
[24] W. Doster, J. Non-Cryst. Solids **357**, 622 (2011).
[25] W. Doster, Eur. Biophys. J. **37**, 591 (2008).
[26] S. H. Chen, L. Liu, E. Fratini, P. Baglioni, A. Faraone, and A. Mamontov, Proc. Natl. Acad. Sci. U.S.A. **103**, 9012 (2006).
[27] T. Becker, J. Hayward, J. L. Finney, R. Daniel, and J. C. Smith, Biophys. J. **87**, 1436 (2004).
[28] F. Gabel, Eur. Biophys. J. **34**, 1 (2005).
[29] G. Kneller and V. Calandrini, J. Chem. Phys. **126**, 125107 (2007).
[30] W. Doster, M. Diehl, W. Petry, and M. Ferrand, Physica B **301**, 65 (2001).
[31] W. Doster, M. Diehl, R. Gebhardt, R. E. Lechner, and J. Pieper, Chem. Phys. **292**, 487 (2003).
[32] M. Bee, *Quasielastic Neutron Scattering* (Adam Hilger, 1988), pp. 28–66.
[33] A. Gaspar, M. S. Appavou, S. Busch, T. Unruh, and W. Doster, BBA **1804**, 76 (2010).
[34] G. L. Squires, *Introduction to the Theory of Thermal Neutron Scattering*, Dover Books in Physics (Dover Publications, Mineola, New York, 1978).
[35] J. P. Boon and S. Yip, *Molecular Hydrodynamics* (Dover Publications, 1980).
[36] N. Niimura, in *Neutron Scattering in Biology*, edited by J. Fitter, T. Gutberlet, and J. Katsaras (Springer, 2006), p. 43.
[37] W. Götze and L. Sjögren, Rep. Prog. Phys. **55**, 241 (1992).
[38] W. Götze and L. Sjögren, Chem. Phys. **212**, 47 (1996).
[39] M. Fuchs, I. Hofacker, and A. Latz, Phys. Rev. A **45**, 898 (1992).
[40] M. Settles and W. Doster, Faraday Discuss. **103**, 269 (1996).
[41] J. Wuttke, Rev. Sci. Instrum. **83**, 107101 (2012).
[42] D. C. Champeney and F. W. D. Woodhams, J. Phys. B **1**, 620 (1968).
[43] F. Parak and E. W. Knapp, Proc. Natl. Acad. Sci. U.S.A. **81**, 7088 (1984).
[44] H. Lichtenegger, W. Doster, T. Kleinert, A. Birk, B. Sepiol, and G. Vogl, Biophys. J. **76**, 414 (1999).
[45] Th. Kleinert, W. Doster, H. Leyser, W. Petry, V. Schwarz, and M. Settles, Biochemistry **37**, 717 (1998).
[46] Y. H. Jeong and S. Nagel, Phys. Rev. A **34**, 602 (1986).
[47] W. Doster, S. Busch, A. Gaspar, M. S. Appavou, J. Wuttke, and J. Scheer, Phys. Rev. Lett. **104**, 098101 (2010).
[48] M. Vogel, Phys. Rev. Lett. **101**, 225701 (2008).
[49] H. Jansson and J. Swenson, BBA Proteins Proteomics **1804**, 20 (2010).
[50] J. Roh, V. N. Novikov, R. B. Gregory, J. E. Curtis, Z. Chowdhuri, and A. P. Sokolov, Phys. Rev. Lett. **95**, 038101 (2005).

[51]G. R. Kneller, S. Cusack, W. Doster, M. Settles, and J. Smith, J. Chem. Phys. **97**, 8864 (1992).
[52]M. Settles and W. Doster, in *Biological Macromolecular Dynamics*, edited by S. Cusack, H. Büttner, M. Ferrand, P. Lagan, and P. Timmins (Adenine Press, NY, USA, 1997), p. 3.
[53]J. Wuttke, W. Petry, and F. Fujara, Phys. Rev. E **52**, 4026 (1995).
[54]F. Fujara, W. Petry, R. M. Diehl, W. Schnauss, and H. Stillescu, Europhys. Lett. **14**, 563 (1991).
[55]W. Doster, Physica B **385–386**, 831 (2006).
[56]S. Cusack and W. Doster, Biophys. J. **58**, 243 (1990).
[57]See supplementary material at http://dx.doi.org/10.1063/1.4816513 for Table II.